JOURNAL OF BACTERIOLOGY, Dec. 2007, p. 8626–8635 Vol. 189, No. 23
0021-9193/07/$08.00+0 doi:10.1128/JB.00777-07

Biochemical Characterization of dTDP-D-Qui4N and dTDP-D-Qui4NAc Biosynthetic Pathways in *Shigella dysenteriae* Type 7 and *Escherichia coli* O7▽†

Ying Wang,[1,2,3] Yanli Xu,[1,2,3] Andrei V. Perepelov,[4] Yuanyuan Qi,[1,2] Yuriy A. Knirel,[4] Lei Wang,[1,2,3] and Lu Feng[1,2,3]*

TEDA School of Biological Sciences and Biotechnology, Nankai University,[1] Tianjin Key Laboratory of Microbial Functional Genomics,[2] and Tianjin Research Center for Functional Genomics and Biochip,[3] 23 Hongda Street, TEDA, Tianjin 300457, People's Republic of China, and N. D. Zelinsky Institute of Organic Chemistry, Russian Academy of Sciences, 119991 Moscow, Russian Federation[4]

Received 18 May 2007/Accepted 19 September 2007

O-antigen variation due to the presence of different types of sugars and sugar linkages is important for the survival of bacteria threatened by host immune systems. The O antigens of *Shigella dysenteriae* type 7 and *Escherichia coli* O7 contain 4-(*N*-acetylglycyl)amino-4,6-dideoxy-D-glucose (D-Qui4NGlyAc) and 4-acetamido-4,6-dideoxy-D-glucose (D-Qui4NAc), respectively, which are sugars not often found in studied polysaccharides. In this study, we characterized the biosynthetic pathways for dTDP-D-Qui4N and dTDP-D-Qui4NAc (the nucleotide-activated precursors of D-Qui4NGlyAc and D-Qui4NAc in O antigens). Predicted genes involved in the synthesis of the two sugars were cloned, and the gene products were overexpressed and purified as His-tagged fusion proteins. In vitro enzymatic reactions were carried out using the purified proteins, and the reaction products were analyzed by capillary electrophoresis, electrospray ionization-mass spectrometry, and nuclear magnetic resonance spectroscopy. It is shown that in *S. dysenteriae* type 7 and *E. coli* O7, dTDP-D-Qui4N is synthesized from α-D-glucose-1-phosphate in three reaction steps catalyzed by glucose-1-phosphate thymidyltransferase (RmlA), dTDP-D-glucose 4,6-dehydratase (RmlB), and dTDP-4-keto-6-deoxy-D-glucose aminotransferase (VioA). An additional acetyltransferase (VioB) catalyzes the conversion of dTDP-D-Qui4N into dTDP-D-Qui4NAc in *E. coli* O7. Kinetic parameters and some other properties of VioA and VioB are described and differences between VioA proteins from *S. dysenteriae* type 7 ($VioA_{D7}$) and *E. coli* O7 ($VioA_{O7}$) discussed. To our knowledge, this is the first time that functions of VioA and VioB have been biochemically characterized. This study provides valuable enzyme sources for the production of dTDP-D-Qui4N and dTDP-D-Qui4NAc, which are potentially useful in the pharmaceutical industry for drug development.

Lipopolysaccharide, also known as endotoxin, is the major component of the outer membranes of gram-negative bacteria. It consists of three moieties: lipid A, the core oligosaccharide, and the O-specific polysaccharide (O antigen). The O antigen is composed of a number of repeats of an oligosaccharide unit (O unit). The O unit usually contains 2 to 8 residues from a broad range of monosaccharides and their derivatives (6, 9). The O antigen is one of the most varied cell constituents due to the variation in the types of sugars present, the arrangement of the sugars within the O unit, and the linkages between sugars. More than 180 O-antigen forms have been recognized in *Escherichia coli* (including *Shigella*) (33). The O antigen is a major target of the immune system and bacteriophages, and O-antigen variation is important for bacterial survival and pathogenicity (31). Several studies have indicated that the composition of the O antigen might be an indicator of virulence potential (18), and some O-antigen forms, including that in *E. coli* O7, are most commonly found in pathogenic *E. coli* strains (25). *Shigella* strains are important human pathogens causing diseases such as diarrhea and bacillary dysentery (26). Genes for the synthesis of the O antigen are normally located in a gene cluster which maps between *galF* and *gnd* on the chromosomes of *E. coli* and *Shigella* (32). Many O-antigen gene clusters have been sequenced, with gene functions proposed (http://www.mmb.usyd.edu.au/BPGD/default.htm). Biosynthetic pathways for several O-antigen sugar precursors, such as UDP-L-FucNAc, have been characterized biochemically (15, 16, 22, 27, 30, 36).

The O antigen of *Shigella dysenteriae* type 7 is composed of a tetrasaccharide O unit containing a residue of 4-(*N*-acetylglycyl)amino-4,6-dideoxy-D-glucose (D-Qui4NGlyAc) (17). The same O-antigen structure is also present in *E. coli* O121, which belongs to Shiga toxin-producing *E. coli* causing hemolytic uremic syndrome (28, 38). The *E. coli* O7 O antigen is composed of a pentasaccharide O unit containing a residue of 4-acetamido-4,6-dideoxy-D-glucose (D-Qui4NAc) (19). Both Qui4NGlyAc and Qui4NAc belong to dideoxy(acetylglycyl/acetyl)amino hexoses, which are sugars not often found in studied polysaccharides.

In our previous study, the O-antigen gene cluster of *S. dysenteriae* type 7 was sequenced and three genes from this organism, $rmlA_{D7}$, $rmlB_{D7}$, and $vioA_{D7}$, were proposed to be responsible for the synthesis of dTDP-D-Qui4N (the nucleotide-activated precur-

* Corresponding author. Mailing address: TEDA School of Biological Sciences and Biotechnology, Nankai University, 23 Hongda Street, TEDA, Tianjin 300457, People's Republic of China. Phone: 86-22-66229592. Fax: 86-22-66229596. E-mail: fenglu63@nankai.edu.cn.

† Supplemental material for this article may be found at http://jb.asm.org/.

▽ Published ahead of print on 28 September 2007.

TABLE 1. Strains, plasmids, and primers used in this study

Bacterial strain, plasmid, or primer	Description or sequence[a]	Source[b]
Strains		
G1222	*S. dysenteriae* serotype 7 type strain	IMVS
G1112	*E. coli* O7 type strain	NICPBP
E. coli BL21(DE3)	F^- *ompT* $hsdS_B(r_B^- m_B^-)$ *gal dcm* (DE3)	Novagen
E. coli DH5α	F^- ϕ80*lacZΔM15 endA recA1 hsdR*$(r_K^- m_K^-)$ *supE44 thi-1 gyrA96 relA1* (*lacZYA-argF*)*U169*	TBC
Plasmids		
$pET28a^+$	T7 expression vector, Kan^r	Novagen
pLW1048	$pET28a^+$ containing N-terminally six-histidine-tagged $rmlA_{D7}$ at the EcoRI/XhoI site	This work
pLW1051	$pET28a^+$ containing C-terminally six-histidine-tagged $rmlB_{D7}$ at the NcoI/XhoI site	This work
pLW1049	$pET28a^+$ containing N-terminally six-histidine-tagged $vioA_{D7}$ at the EcoRI/XhoI site	This work
pLW1195	$pET28a^+$ containing N-terminally six-histidine-tagged $vioA_{O7}$ at the BamHI/HindIII site	This work
pLW1155	$pET28a^+$ containing C-terminally six-histidine-tagged $vioB_{O7}$ at the NcoI/SalI site	This work
Primers		AuGCT
wl-4235 (*rmlA*-D7F)	5′-TAGAATTCATGGCTTACTCAGCAGTATG-3′	
wl-4236 (*rmlA*-D7R)	5′-TTGGCTCTCGAGTTATTTGTCCTTAAC-3′	
wl-4241 (*rmlB*-D7F)	5′-GCAGCCATGGAAATCCTTATTACAG-3′	
wl-4242 (*rmlB*-D7R)	5′-GTCCTCGAGTTTCATTTCTCCATACTG-3′	
wl-4243 (*vioA*-D7F)	5′-GAGAATTCATGGAAAAGCCAATCTTTGTAAC-3′	
wl-4244 (*vioA*-D7R)	5′-GCACTTCTCGAGTCATTTAATCTCCCTAATC-3′	
wl-5702 (*vioA*-O7F)	5′-GCAGGATCCATGAACGATAAAACTATTCCAGTAAC-3′	
wl-5703 (*vioA*-O7R)	5′-GTCGAAGCTTTCACATCTTACCCAATAATAATTTG-3′	
wl-4704 (*vioB*-O7F)	5′-GGTCCCATGGCCTATTTAGATGAAATAC-3′	
wl-4705 (*vioB*-O7R)	5′-CGGAAGTCGACCAGATTATCTCCAATAG-3′	

[a] The underlined sequences indicate restriction sites.
[b] IMVS, the Institute of Medical and Veterinary Science, Adelaide, Australia; NICPBP, the National Institute for the Control of Pharmaceutical and Biological Products, Beijing, China; TBC, Tianjin Biochip Corporation, Tianjin, China; AuGCT, AuGCT Biotechnology Corporation, Beijing, China.

sor of D-Qui4NGlyAc) (10). Glucose-1-phosphate thymidyltransferase (RmlA) catalyzes the conversion of glucose-1-phosphate to dTDP-D-glucose (dTDP-D-Glc), which is then converted to dTDP-4-keto-6-deoxy-D-glucose (dTDP-D-Glc4O) by dTDP-D-glucose 4,6-dehydratase (RmlB). Both reaction steps have been biochemically verified in a number of bacterial strains (11, 30). VioA, a putative sugar aminotransferase (SAT) of the DegT/DnrJ/EryC1/StrS family, was proposed to catalyze the conversion of dTDP-D-Glc4O to dTDP-D-Qui4N. The *E. coli* O7 O-antigen gene cluster was also sequenced (20), and the biosynthetic pathway for dTDP-D-Qui4NAc was proposed, in which dTDP-D-Qui4NAc is derived from dTDP-D-Qui4N by a transacetylation reaction catalyzed by a putative acetyltransferase of the NodL-LacA family, $VioB_{O7}$ (20). However, the functions of VioA and VioB have not yet been confirmed.

In this study, we characterized the biosynthetic pathways of dTDP-D-Qui4N and dTDP-D-Qui4NAc. Genes encoding RmlA, RmlB, VioA, and VioB were cloned from *S. dysenteriae* type 7 ($rmlA_{D7}$, $rmlB_{D7}$, and $vioA_{D7}$) and/or *E. coli* O7 ($vioA_{O7}$ and $vioB_{O7}$), and the gene products were overexpressed and purified as His-tagged fusion proteins. In vitro enzymatic reactions were carried out, and the products were analyzed by spectroscopic methods. VioA was identified as a novel aminotransferase catalyzing the conversion of dTDP-D-Glc4O to dTDP-D-Qui4N in *S. dysenteriae* type 7 and *E. coli* O7, and VioB was identified as a novel acetyltransferase catalyzing the conversion of dTDP-D-Qui4N to dTDP-D-Qui4NAc in *E. coli* O7. Enzymatic properties of VioA and VioB were investigated, and differences between $VioA_{D7}$ and $VioA_{O7}$ are discussed.

MATERIALS AND METHODS

Materials. α-D-Glucose-1-phosphate, dTTP, dTDP-D-Glc, pyridoxal-5-phosphate (PLP), inorganic pyrophosphatase, acetyl coenzyme A (acetyl-CoA), SH-CoA, and aminooxy acetic acid were purchased from Sigma-Aldrich (St. Louis, MO), methanol and acetonitrile were purchased from Fisher (Pittsburgh, PA), and acetic acid was purchased from Fluka (Buchs SG, Switzerland). All the chemicals were at the highest purity available. Restriction enzymes and recombinant *Taq* DNA polymerase were from TaKaRa (Japan), and T4 DNA ligase was from Promega (Madison, WI). Other chemicals and reagents were from Sangon Co., Ltd. (Shanghai, China). Bacterial strains and plasmids used are listed in Table 1.

Cloning and plasmid construction. Chromosomal DNA was prepared as previously described (3). The $rmlA_{D7}$, $rmlB_{D7}$, and $vioA_{D7}$ genes were PCR amplified from strain G1222, and the $vioA_{O7}$ and $vioB_{O7}$ genes were amplified from strain G1112. Primers used are listed in Table 1. A total of 30 cycles (25 cycles for $vioA_{O7}$) were performed using the following conditions: denaturation at 95°C for 30 s, annealing at 50°C (55°C for $vioA_{O7}$) for 30 s, and extension at 72°C for 1 min in a final volume of 25 μl. The amplified genes were cloned into $pET28a^+$ to construct plasmids pLW1048 (containing $rmlA_{D7}$), pLW1051 (containing $rmlB_{D7}$), pLW1049 (containing $vioA_{D7}$), pLW1195 (containing $vioA_{O7}$), and pLW1155 (containing $vioB_{O7}$) (Table 1), and the inserts were sequenced by Tianjin Biochip Cooperation using an ABI 3730 sequencer.

Protein expression and purification. *E. coli* BL21(DE3) carrying each of the recombinant plasmids was grown overnight at 37°C in LB medium containing 50 μg/ml kanamycin. The overnight culture (5 ml) was inoculated into 500 ml of fresh LB medium and grown until the A_{600} reached 0.6. The expression of $RmlA_{D7}$, $VioA_{D7}$, and $VioB_{O7}$ was induced with 0.1 mM isopropyl-β-D-thiogalactopyranoside (IPTG) at 37°C for 4 h, and expression of $RmlB_{D7}$ and $VioA_{O7}$ was induced with 0.1 mM IPTG at 12°C for 8 h and at 25°C for 4 h. After IPTG induction, cells were harvested by centrifugation, washed with 50 mM Tris-HCl (pH 8.0) containing 300 mM NaCl and 10 mM imidazole, resuspended into 5 ml of the same buffer, and sonicated. The cell debris was removed by centrifugation, and total soluble proteins in the supernatant were collected. The His_6-tagged fusion proteins in the supernatant were purified by nickel ion affinity chromatography with a chelating Sepharose Fast Flow (GE

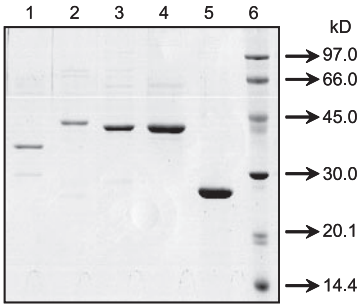

FIG. 1. SDS-polyacrylamide gel electrophoresis of purified $RmlA_{D7}$ (lane 1), $RmlB_{D7}$ (lane 2), $VioA_{D7}$ (lane 3), $VioA_{O7}$ (lane 4), and $VioB_{O7}$ (lane 5). Proteins were denatured at 100°C for 5 min in 0.1% SDS and 1% 2-mercaptoehanol before being loaded in a 5% (wt/vol) stacking gel and separated in a 12% (wt/vol) separation gel. The gel was stained with Coomassie bright blue R250. The molecular weight markers from the LMW-SDS marker kit (GE Healthcare) are indicated at the right of the panel.

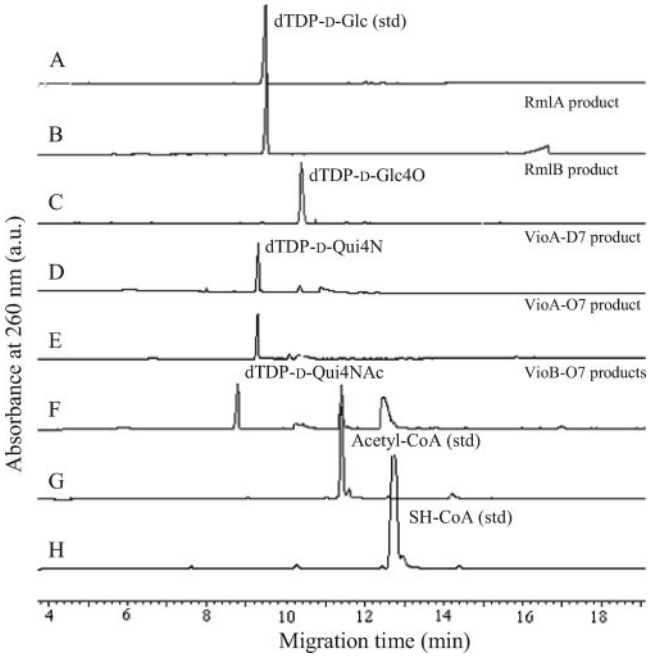

FIG. 2. CE chromatographs of reaction products. Shown are chromatographs of standard (std) dTDP-D-Glc without addition (A) and after the addition of $RmlA_{D7}$ (B); $RmlA_{D7}$ and $RmlB_{D7}$ (C); $RmlA_{D7}$, $RmlB_{D7}$, and $VioA_{D7}$ (D); $RmlA_{D7}$, $RmlB_{D7}$, and $VioA_{O7}$ (E); $RmlA_{D7}$, $RmlB_{D7}$, $VioA_{O7}$, and $VioB_{O7}$ (F); standard acetyl-CoA (G); and standard SH-CoA (H). a.u., arbitrary units.

Healthcare) column according to the manufacturer's instructions. Unbound proteins were washed out with 100 ml of wash buffer (50 mM Tris-HCl, pH 8.0, 300 mM NaCl, and 25 mM imidazole). The fusion proteins were eluted with 3 ml of elution buffer (50 mM Tris-HCl, pH 8.0, 300 mM NaCl, and 250 mM imidazole) and dialyzed overnight against 50 mM potassium phosphate buffer (pH 7.4) at 4°C. Protein concentration was determined by the Bradford method.

Enzyme activity assays. The reaction mixture for RmlA contained 50 mM potassium phosphate buffer (pH 7.4), 5 mM $MgCl_2$, 4 mM α-D-glucose-1-phosphate, 4 mM dTTP, 0.02 U inorganic pyrophosphatase, and a 0.13 μM concentration of purified $RmlA_{D7}$ (39). The reaction mixture for RmlB contained 50 mM potassium phosphate buffer (pH 7.4), 5 mM $MgCl_2$, 8 mM dTDP-D-Glc, and a 2.65 μM concentration of purified $RmlB_{D7}$ (39). To assay the VioA activity, the RmlB mixture was supplemented with 50 mM L-glutamate (L-Glu), 0.2 mM PLP, and 2 μM $VioA_{D7}$ or 0.66 μM $VioA_{O7}$ after the RmlB reaction (30). To assay the VioB activity, the VioA mixture was supplemented with 2.5 mM acetyl-CoA and 1.93 μM $VioB_{O7}$ after the VioA reaction (30). All reactions were carried out in a final volume of 50 μl at 37°C for 2 h unless otherwise indicated. Products from each of the reactions were analyzed by capillary electrophoresis (CE), electrospray ionization mass spectrometry (ESI-MS), and nuclear magnetic resonance spectroscopy (NMR). Enzyme activities were indicated by the conversion of substrates into products.

Kinetic-parameter measurements. To measure K_m and V_{max} values of $VioA_{D7}$ and $VioA_{O7}$, reactions were carried out with various concentrations of dTDP-D-Glc4O (0.05 to 2 mM for $VioA_{D7}$ and 0.02 to 0.1 mM for $VioA_{O7}$) with 1 μM $VioA_{D7}$ and 0.022 μM $VioA_{O7}$. To measure K_m and V_{max} values of VioB, reactions were carried out with various concentrations of dTDP-D-Qui4N (0.08 to 0.48 mM), a constant concentration of acetyl-CoA (3 mM), various concentrations of acetyl-CoA (0.187 to 1.87 mM), and a constant concentration of dTDP-D-Qui4N (1.9 mM) with a 3.86 nM concentration of purified $VioB_{O7}$. All reactions were performed in a final volume of 20 μl, and reactions were terminated by adding an equal volume of chloroform. Conversion from dTDP-D-Glc4O to dTDP-D-Qui4N and from dTDP-D-Qui4N to dTDP-D-Qui4NAc was examined by CE. Conversion of acetyl-CoA to SH-CoA was measured with Ellman's reagent according to the method of Pfoestl et al. (30). K_m and V_{max} values were calculated based on the Michaelis-Menten equation. The data are averages of results from three independent experiments.

Determination of temperature optimum, divalent-cation effects, and amino donor requirements for $VioA_{D7}$, $VioA_{O7}$, and $VioB_{O7}$. To determine the temperature optimum for each enzyme, reactions were carried out at 4, 15, 25, 37, 50, 65, and 75°C, respectively. To test the effects of different cations on enzyme activity, reactions were carried out in the presence of 5 mM $MgCl_2$, $MnCl_2$, $FeSO_4$, $CoCl_2$, and $CaCl_2$ for 1 h ($VioA_{D7}$), 30 min ($VioA_{O7}$), or 20 min ($VioB_{O7}$). To test the amino donors for the transamination reactions catalyzed by $VioA_{D7}$ and $VioA_{O7}$, reactions were carried out in the presence of 50 mM L-arginine (L-Arg), L-aspartic acid (L-Asp), L-asparagine (Asn), L-glycine (L-Gly), L-alanine (L-Ala), L-glutamine (L-Gln), or L-Glu. Enzyme activities were examined by CE, and the data are the averages of results from three independent experiments.

CE. CE was performed using a Beckman Coulter P/ACE MDQ CE system with a photoelectricity diode array detector (Beckman Coulter, CA). The capillary was bare silica (inside diameter, 75 μm by 57 cm, with the detector at 50 cm) and conditioned before each run by washing it with 0.1 M NaOH first, with deionized water next, and with 25 mM borate-sodium hydroxide, pH 9.4 (used as the mobile phase) last for 2 min each time. Samples were loaded by pressure injection at 0.5 lb/in^2 for 10 s, and separation was carried out at 20 kV. Peak integration and trace alignments were done with Beckman P/ACE Station software (32 Karat, version 5.0). Conversion ratios were calculated by comparing the peak areas of the substrate and product.

ESI-MS and tandem MS. The reaction mixtures of $RmlB_{D7}$, $VioA_{D7}$, and $VioB_{O7}$ were separated by reverse-phase high-performance liquid chromatography (RP-HPLC) using a BioCAD 700E perfusion chromatography workstation (Applied Biosystems, CA) with an Venusil MP-C18 column (5-μm particle size, 4.6 by 250 mm) (Agela Technologies, Inc.). The mobile phase used was composed of 10% acetonitrile and 90% 50 mM triethylamine-acetic acid (pH 6.0), and the flow rate was 0.6 ml/min. Fractions containing the expected products were collected, lyophilized, and redissolved in 50% methanol before they were injected into a Finnigan LCQ Advantage MAX ion trap mass spectrometer (Thermo Electron, CA) in the negative mode (4.5 kV, 250°C) for ESI-MS analysis. For second and third MS (MS2 and MS3) analyses, nitrogen was used as the collision gas and helium as the auxiliary gas and collision energies used were typically 20 to 30 eV.

NMR spectroscopy. A sample of dTDP-D-Qui4NAc (0.2 mg) was deuterium exchanged by freeze-drying from D_2O, dissolved in 99.96% D_2O (150 μl), and examined using a Shigemi (Japan) microtube. NMR spectra were recorded on a Bruker DRX-500 spectrometer (Germany) at 30°C using internal sodium trimethylsilyl- [2,2,3,3-$^2H_4$]propanoate (δ_H 0.00) and external aqueous 85% H_3PO_4 (δ_P 0) as references. Two-dimensional NMR spectra were obtained using standard pulse sequences from the manufacturer, and the XWinNMR 2.6 program (Bruker) was used to acquire and process the NMR data. A mixing time of 200 ms was used in a *to*tal *c*orrelation *s*pectroscop*y* (TOCSY) experiment, which was employed to correlate all coupled protons within each spin system (4).

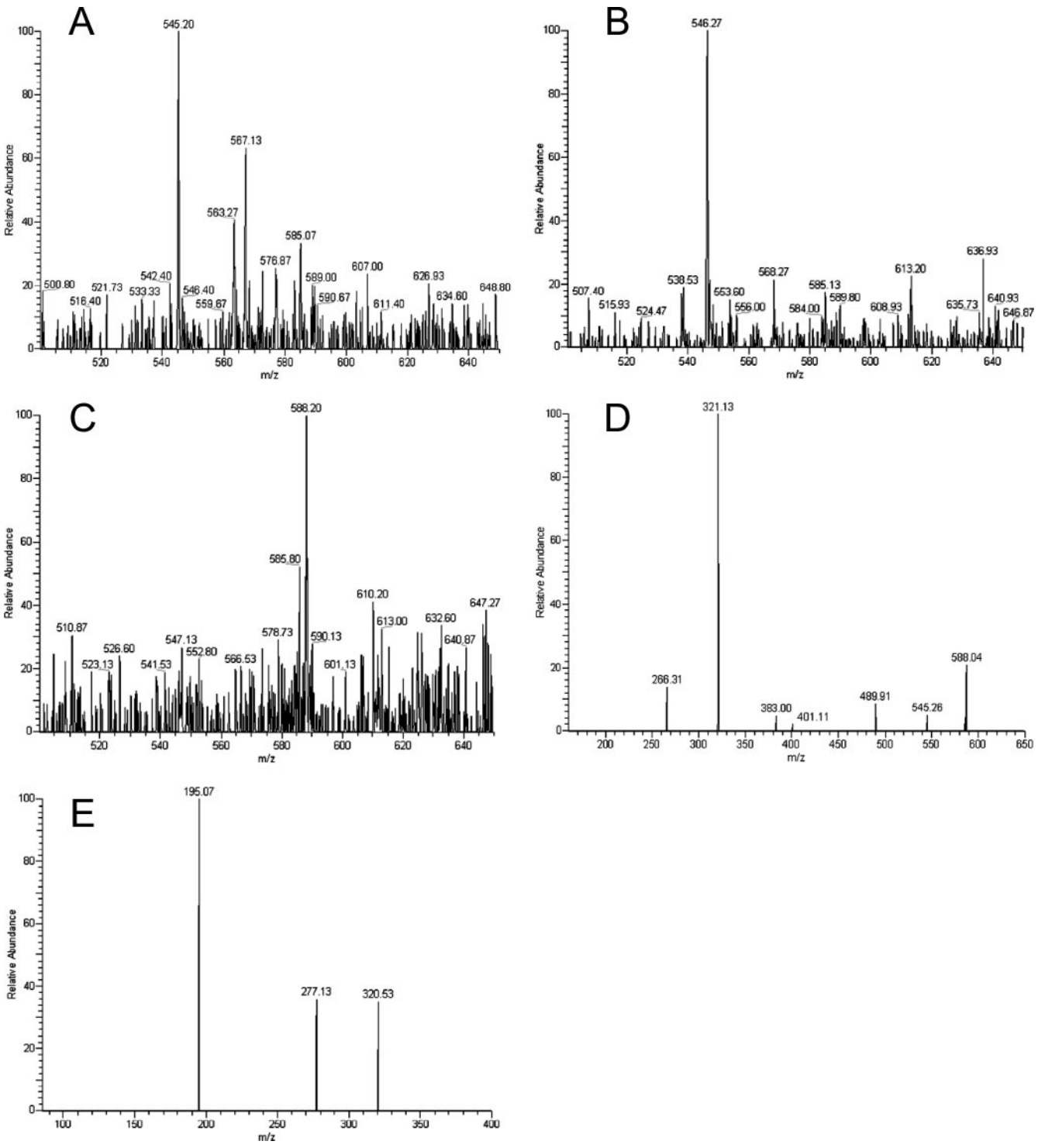

FIG. 3. ESI-mass spectra of dTDP-D-Glc4O (A), dTDP-D-Qui4N (B), and dTDP-D-Qui4NAc (C); MS2 analysis of the ion with *m/z* 588.20 in panel C (D); and MS3 analysis of the ion with *m/z* 321.13 in panel D (E).

RESULTS

Overexpression and purification of enzymes. Plasmids pLW1048 (containing $rmlA_{D7}$), pLW1051 (containing $rmlB_{D7}$), pLW1049 (containing $vioA_{D7}$), pLW1195 (containing $vioA_{O7}$), and pLW1155 (containing $vioB_{O7}$) were constructed, and the expression of each of the five genes in *E. coli* BL21(DE3) carrying the corresponding plasmids was induced by IPTG as described in Materials and Methods. The majority of each protein was found in the soluble fraction (data not shown), and the proteins were purified to near homogeneity by nickel

ion affinity chromatography (Fig. 1). The apparent molecular masses of histidine-tagged $RmlA_{D7}$, $RmlB_{D7}$, $VioA_{D7}$, $VioA_{O7}$, and $VioB_{O7}$ estimated by sodium dodecyl sulfate (SDS)-polyacrylamide gel electrophoresis analysis were 38.3, 45.6, 43.7, 43.8, and 27.1 kDa, respectively, correlating well with the predicted molecular masses (36.1, 42.3, 42.5, 45.2, and 22.4 kDa).

In vitro characterization of dTDP-D-Qui4N and dTDP-D-Qui4NAc biosynthetic pathways by CE. Biosynthetic pathways of dTDP-D-Qui4N and dTDP-D-Qui4NAc were characterized by carrying out each of the enzymatic steps sequentially in a single reaction mixture containing α-D-glucose-1-phosphate as the initial substrate and by analyzing each of the reaction products by CE. When $RmlA_{D7}$, the first enzyme of the pathways, was added, a peak eluted at the same time (9.5 min) that the standard dTDP-D-Glc (Fig. 2A and B) was produced, confirming the function of $RmlA_{D7}$ as RmlA. When the second enzyme, $RmlB_{D7}$, was added, the peak corresponding to dTDP-D-Glc was converted to a peak that eluted at 10.4 min, indicating that the emerging peak is the product of RmlB (Fig. 2C). The peak at 10.4 min was converted to a new peak that eluted at 9.3 min when L-glutamate, PLP, and purified $VioA_{D7}$ were added next (Fig. 2D), and this peak had not appeared when $VioA_{D7}$ was heat denatured before the addition or in the presence of the PLP-dependent aminotransferase inhibitor aminooxy acetic acid (12; data not shown). The same was found when purified $VioA_{O7}$ was used instead of $VioA_{D7}$ (Fig. 2E). These results indicated that the peak at 9.3 min was the product of $VioA_{D7}$ and $VioA_{O7}$ and that both enzymes are PLP-dependent aminotransferases catalyzing the transfer of an amino group onto the RmlB product. The peak at 9.3 min disappeared almost completely, and another new peak that migrated at 8.8 min appeared when acetyl-CoA and purified $VioB_{O7}$ were added to the reaction mixture (Fig. 2F). Conversion of acetyl-CoA to SH-CoA was also detected by comparing the migration times of the peaks before and after the reaction with those of the standard chemicals (Fig. 2G and H), indicating that the acetyl group was transferred to the VioA product. No products were produced when $VioB_{O7}$ was heat denatured before the addition (data not shown).

Structural identification of the reaction products by ESI-MS and tandem MS. Products of $RmlB_{D7}$, $VioA_{D7}$, and $VioB_{O7}$ were separated and purified by RP-HPLC (data not shown). Fractions containing each of the RmlB, VioA, and VioB products were collected and analyzed by ESI-MS (Fig. 3A to C). Ion peaks at *m/z* 545.20 (Fig. 3A), 546.27 (Fig. 3B), and 588.20 (Fig. 3C) were obtained, which are in agreement with the expected masses for dTDP-D-Glc4O (*m/z* 544.32), dTDP-D-Qui4N (*m/z* 547.34), and dTDP-D-Qui4NAc (*m/z* 589.38). Ion peaks representing each sugar plus one or two Na^+ ions were also detected (Fig. 3A to C; Table 2).

Further analyses by MS2 and MS3 were performed to confirm the molecular mass of the $VioB_{O7}$ product, the end product of the Qui4NAc biosynthetic pathway. MS2 analysis of the product peak at *m/z* 588.20 produced peaks at *m/z* 545.26, 401.11, 383.00, and 321.13, matching the masses of the dTDP-D-Qui4NAc minus acetyl group, dTDP-H_2O, dTDP, and the Qui4NAc-PO_3-PO_3 minus acetyl group, respectively. Peaks corresponding to dTDP-D-Qui4NAc minus CH_3-CO-NH-CH-CH-CH_3 (*m/z* 489.91) and Qui4NAc-PO_3-PO_3 minus CH_3-CO-NH-CH-CH-CH_3 (*m/z* 266.31) resulting from fragmentation of the hexose rings between C-3–C-4 and C-5–O were also detected (Fig. 3D; Table 2). When the ion peak at *m/z* 321.13 was selected as a parent peak for MS3 analysis, a peak at *m/z* 277.13, which matched the fragment of Qui4NAc-PO_3-PO_3 minus acetyl and CH_3-CH-O, resulted from fragmentation of the hexose rings between C-4–C-5 and O–C-1 (Fig. 3E; Table 2). These results indicated that an acetamido group had been added to the C-4 position of the glucose moiety of the $VioB_{O7}$ product, confirming the identity of Qui4NAc as the product of $VioB_{O7}$. Fragments corresponding to each peak are depicted in Table 2.

TABLE 2. Interpretations of the ion peaks shown in Fig. 3

Composition of fragment	Molecular formula	Molecular wt	Mass (negative)
dTDP-D-Glc4O (full scan)			
dTDP-D-Glc4O-Na_2	$C_{16}H_{22}P_2O_{15}N_2Na_2$	590.27	589.00
dTDP-D-Glc4O-Na	$C_{16}H_{23}P_2O_{15}N_2Na$	568.29	567.13
dTDP-D-Glc4O	$C_{16}H_{22}P_2O_{15}N_2$	544.32	545.20
dTDP-D-Qui4N (full scan)			
dTDP-D-Qui4N-Na_2	$C_{16}H_{25}P_2O_{14}N_3Na_2$	591.31	589.80
dTDP-D-Qui4N-Na	$C_{16}H_{25}P_2O_{14}N_3Na$	569.32	568.27
dTDP-D-Qui4N	$C_{16}H_{27}P_2O_{14}N_3$	547.34	546.27
dTDP-D-Qui4NAc(full scan)			
dTDP-D-Qui4NAc-Na_2	$C_{18}H_{27}P_2O_{15}N_3Na_2$	633.34	632.60
dTDP-D-Qui4NAc-Na	$C_{18}H_{28}P_2O_{15}N_3Na$	611.35	610.20
dTDP-D-Qui4NAc	$C_{18}H_{29}P_2O_{15}N_3$	589.38	588.20[a]
dTDP-D-Qui4NAc (MS2, 588.20)			
dTDP-D-Qui4NAc minus acetyl group	$C_{16}H_{26}P_2O_{14}N_3$	546.32	545.26
dTDP-D-Qui4NAc minus CH_3-CO-NH-CH-CH-CH_3	$C_{13}H_{20}P_2O_{14}N_2$	490.25	489.91
dTDP plus H_2O	$C_{10}H_{15}P_2O_{11}N_2$	401.18	401.11
dTDP	$C_{10}H_{13}P_2O_{10}N_2$	383.16	383.00
Qui4NAc-PO_3-PO_3 minus acetyl group	$C_6H_{14}P_2O_{10}N$	322.12	321.13[a]
Qui4NAc-PO_3-PO_3 minus CH_3-CO-NH-CH-CH-CH_3	$C_3H_8P_2O_{10}$	266.04	266.31
dTDP-D-Qui4NAc (MS3, 321.13)			
Qui4NAc-PO_3-PO_3 minus acetyl and CH_3-CH-O	$C_4H_{10}P_2O_9N$	278.07	277.13
PO_3-PO_3-$2H_2O$	$P_2O_8H_6$	195.99	195.07

[a] The ESI-mass peaks at *m/z* 588.20 and 321.13 were selected as parent ions for MS2 and MS3, respectively.

Determination of the configuration at C-4 of the hexose unit in the $VioB_{O7}$ product by NMR spectroscopy. The ^1H NMR spectrum of dTDP-D-Qui4NAc was assigned using two-dimensional ^1H,^1H COSY and TOCSY experiments. In the TOCSY spectrum (Fig. 4), cross-peaks were generated between all coupled protons within each spin system, including those between H-1 and H-2–H-6 of the QuiNAc moiety at δ 5.58 (H-1)/3.61 (H-2), 3.77 (H-3), 3.63 (H-4), 4.06 (H-5), and 1.18 (H-6);

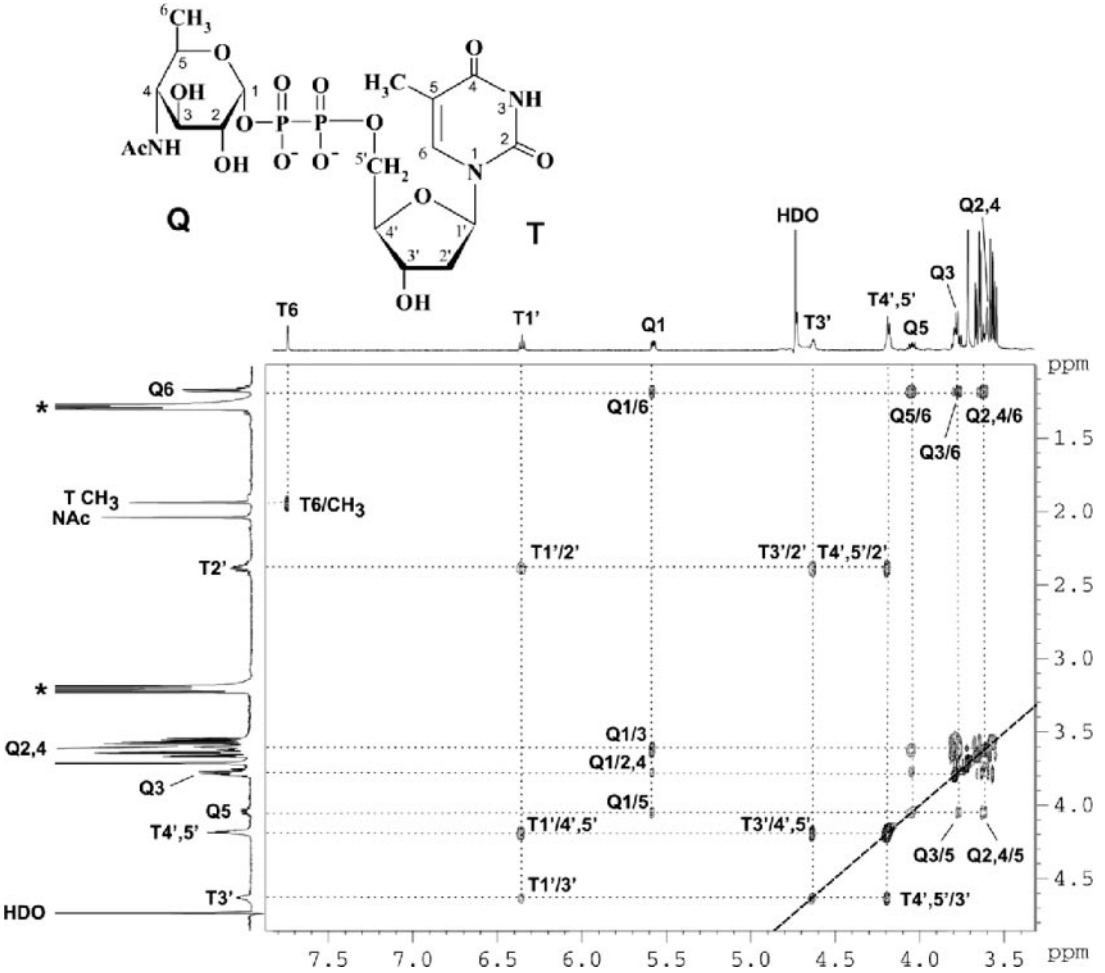

FIG. 4. Part of a $^{1}H,^{1}H$ TOCSY spectrum of dTDP-D-Qui4NAc. The corresponding parts of the ^{1}H NMR spectrum are displayed along the axes. Arabic numerals refer to protons in the Qui4NAc and dTDP moieties designated Q and T, respectively. Signals of contaminating triethylamine are marked with an asterisk. Connectivities between coupled protons in the spin systems of Qui4NAc (Q1-Q6), 2′-deoxyribose (T1′-T5′), and thymine (T6-CH_3) are traced by dotted lines. The structure of dTDP-D-Qui4NAc, the enzymatic product of $VioB_{O7}$, is shown.

between H-1′ and H-2′–H-5′ of 2′-deoxyribose in the dTDP moiety at δ 6.35 (H-1)/2.38 (H-2), 4.63 (H-3), and 4.18 (H-4–H-5a and –H-5b); and between H-6 and CH_3 of thymine at δ 7.74/1.93. The assigned chemical shifts were in good agreement with those published for dTDP (24) and α-Qui4NAc (29). Relatively large $^{3}J_{2,3}$, $^{3}J_{3,4}$, and $^{3}J_{4,5}$ coupling constants (ca. 9 to 10 Hz) determined from the ^{1}H NMR spectrum are characteristic for the all-axial orientation of the Qui4NAc ring protons; hence, the sugar has the *gluco* configuration and is thus 4-acetamido-4,6-dideoxy-α-D-glucose. The ^{31}P NMR spectrum contained signals for a diphosphate group at δ −11.1 and −12.7, which, as expected, showed strong correlations with the H-5′ signal of dTDP at δ −11.1/4.18 and H-1 of α-Qui4NAc at δ −12.7/5.58 in the $^{1}H,^{31}P$ heteronuclear multiquantum coherence spectrum. These data proved finally that the enzymatic product of $VioB_{O7}$ is dTDP-D-QuiNAc, whose structure is depicted in Fig. 4. The biosynthetic pathways for dTDP-D-Qui4N and dTDP-D-Qui4NAc are summarized in Fig. 5.

Kinetic parameters for $VioA_{D7}$, $VioA_{O7}$, and $VioB_{O7}$. Kinetic parameters for the three enzymes investigated are listed in Table 3. The kinetics of the reactions catalyzed by $VioA_{D7}$, $VioA_{O7}$, and $VioB_{O7}$ fit reasonably well to the Michaelis-Menten model (Fig. S1 in the supplemental material). The K_m values for dTDP-D-Glc4O of $VioA_{D7}$ and $VioA_{O7}$ are 980 μM and 45.8 μM, respectively, and the K_m values of $VioB_{O7}$ are 142 μM for dTDP-D-Qui4N and 554 μM for acetyl-CoA (Table 3).

Determination of temperature optimum and shelf life for $VioA_{D7}$, $VioA_{O7}$, and $VioB_{O7}$. Activities of $VioA_{D7}$, $VioA_{O7}$, and $VioB_{O7}$ at temperatures ranging from 4 to 75°C are shown in Fig. 6A. Different temperature effects were observed for $VioA_{D7}$ and $VioA_{O7}$. For $VioA_{O7}$, the conversion rate increased along with a rise in temperature and reached to 90.3% at 75°C. For $VioA_{D7}$, the conversion rate was highest (90.7%) at 37°C and greatly decreased at 65°C and above. At lower temperatures ranging from 4 to 25°C, the conversion rate for $VioA_{O7}$ was much lower than for $VioA_{D7}$. $VioB_{O7}$ showed high activity over a wide temperature range from 4 to 65°C, with complete conversion at temperatures of 25, 37, and 50°C (Fig. 6A). Conversion rates at temperatures above 75°C were not tested due to the instability of nucleotide-activated sugars at high temperatures, as indicated by the detection of the

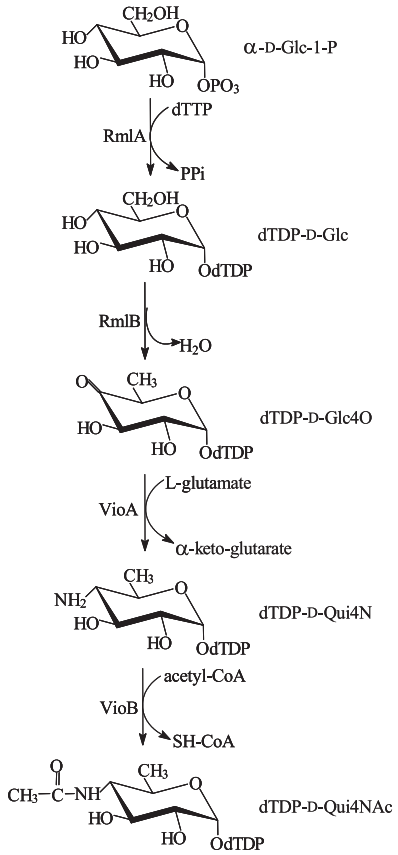

FIG. 5. Pathways for the biosynthesis of dTDP-D-Qui4N and dTDP-D-Qui4NAc. α-D-Glc-1-P, α-D-glucose-1-phosphate; PPi, inorganic pyrophosphate.

breakdown products by CE (data not shown). After being preserved in 50% glycerol for 2 months at −80°C, no significant loss of activity was observed for $VioA_{D7}$, $VioA_{O7}$, and $VioB_{O7}$.

Effects of divalent cations on the completion of enzyme-substrate reactions. The effects of divalent cations, including Mg^{2+}, Ca^{2+}, Mn^{2+}, Fe^{2+}, and Co^{2+}, on the activities of $VioA_{D7}$, $VioA_{O7}$, and $VioB_{O7}$ are shown in Fig. 6B. For $VioA_{D7}$ and $VioA_{O7}$, Mg^{2+} had no effects on the activities of both enzymes, but other cations tested showed different levels of inhibition of the activities, with Co^{2+} being the strongest inhibitor. $VioA_{O7}$ was more prone to divalent-cation inhibition than $VioA_{D7}$, with the rate of conversion in the presence of Co^{2+} being only 3.9%, compared with 22.2% for $VioA_{D7}$. For $VioB_{O7}$, complete conversion was obtained in the absence of cations and in the presence of Mg^{2+}, Ca^{2+}, Mn^{2+}, and Co^{2+}; however, the conversion rate

TABLE 3. Kinetic parameters

Enzyme	Substrate	K_m (μM)	V_{max} (μM/s)	k_{cat}/s
$VioA_{D7}$	dTDP-D-Glc4O	980 ± 157	0.74 ± 0.42	0.74 ± 0.42
$VioA_{O7}$	dTDP-D-Glc4O	45.8 ± 7.3	0.125 ± 0.009	5.66 ± 0.41
$VioB_{O7}$	SH-CoA	554 ± 73	0.953 ± 0.059	21.6 ± 1.3
$VioB_{O7}$	dTDP-D-Qui4N	142 ± 15	0.601 ± 0.159	155.3 ± 41.4

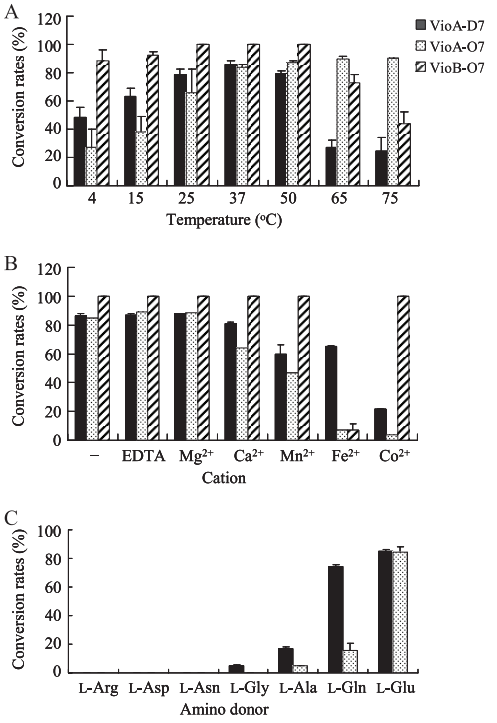

FIG. 6. Effects of temperature (A), cations (B), and amino donors (C) on the conversion rates of $VioA_{D7}$, $VioA_{O7}$, and $VioB_{O7}$.

obtained in the presence of Fe^{2+} was only 4.2%, indicating that all cations tested except for Fe^{2+} have no effects on the activity of $VioB_{O7}$. The inhibition of all cations was released when EDTA as the cation-chelating agent was added (data not shown). All those indicate that all three enzymes are divalent cation independent. EDTA also had no effect on the activities of all three enzymes (Fig. 6B).

Analysis of amino donors for $VioA_{D7}$ and $VioA_{O7}$. Seven amino acids, including L-Arg, L-Asp, L-Asn, L-Gly, L-Ala, L-Gln, and L-Glu, were tested as amino donors for the transamination reaction catalyzed by $VioA_{D7}$ and $VioA_{O7}$ (Fig. 6C). High conversion rates for both $VioA_{D7}$ (84.9%) and $VioA_{O7}$ (84.5%) were obtained when L-Glu was utilized, and this is consistent with other PLP-dependent SATs (12). L-Gln was also an effective amino donor for $VioA_{D7}$, with a 74.1% conversion rate being detected, but less effective for $VioA_{O7}$ (15.9%). In addition, L-Ala could be used by both VioA enzymes and L-Gly by only $VioA_{D7}$ as poor amino donors.

DISCUSSION

This is the first report on the characterization of the biosynthetic pathways for dTDP-D-Qui4N and dTDP-D-Qui4NAc. Genes encoding enzymes for all four reaction steps were functionally confirmed by in vitro experiments. Until now, functions of VioA and VioB have not unambiguously been defined. An early study reported purification of a SAT from *E. coli* strain B for the conversion of TDP-D-Glc4O to TDP-D-Qui4N; however, no structural verification of the enzyme product was carried out, and a putative gene was not proposed (21). RmlA and RmlB catalyzing the first two steps of the pathways have

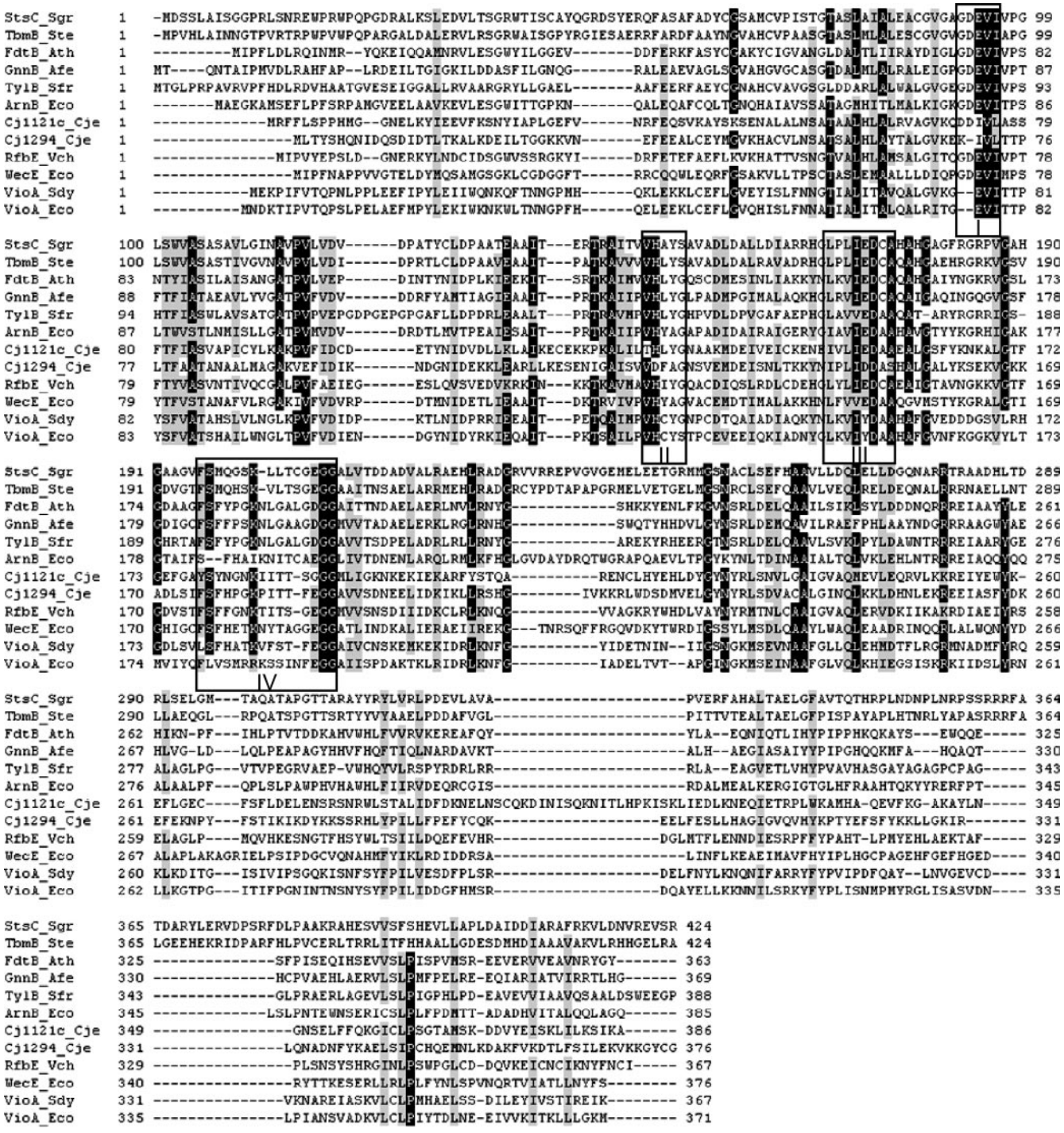

FIG. 7. Sequence alignments of $VioA_{D7}$, $VioA_{O7}$, and other reported sugar aminotransferases. Multiple alignments were performed with the Clustal W program using the BioEdit sequence alignment software. The GenBank accession numbers for StsC_Sgr, TbmB_Ste, FdtB_Ath, GnnB_Afe, TylB_Sfr, ArnB_Eco, Cj1121c_Cje, Cj1294_Cje, RfbE_Vch, WecE_Eco, VioA_Sdy, and VioA_Eco are CAA70012, Q2MF17, AAS55722, AAS48422, S49052, AAM92146, CAL35238, AAT12282, CAA42137, AAC76796, AAR97958, and AAD44154, respectively. Four motifs are boxed. Sgr, *Streptomyces griseus*; Ste, *Streptomyces tenebrarius*; Ath, *Aneurinibacillus thermoaerophilus*; Afe, *Acidithiobacillus ferrooxidans*; Sfr, *Streptomyces fradiae*; Eco, *Escherichia coli*; Cje, *Campylobacter jejuni*; Vch, *Vibrio cholerae*; Sdy, *Shigella dysenteriae*.

been functionally identified in several other bacterial species (11, 30). In this study, we confirmed the functions of RmlA and RmlB from *S. dyenteriae* type 7 and utilized those two enzymes to produce the substrate (dTDP-D-Glc4O) for the assay of VioA. The product of the VioA reaction was then used as the substrate (dTDP-D-Qui4N) for the VioB reaction. Neither of the two substrates is commercially available. Accordingly, concentrations of those two chemicals were calculated based on

conversion rates of the substrates from the previous reaction steps.

$VioA_{D7}$ and $VioA_{O7}$ catalyze the same transamination reaction. Sequence analysis reveals that the two SATs share 53% identity (67% similarity), which is much higher than the levels they share with other reported SATs (Table S1 in the supplemental material). Based on the position of the amino receptor, SATs can be divided into three subgroups acting on *scyllo*-inosose (1, 13, 14), NDP-3-keto sugars (7, 23, 30, 35), or NDP-4-keto sugars (2, 5, 12, 27, 34, 36). This is also supported by the phylogenetic analysis of SATs (Fig. S2 in the supplemental material). As expected, $VioA_{D7}$ and $VioA_{O7}$ fall into the NDP-4-keto sugar subgroup but form a separate branch within the subgroup in the phylogenetic tree.

Sequence alignment of $VioA_{D7}$, $VioA_{O7}$, and other reported SATs reveals the substitution of amino acids at the potential activity sites in motifs II and IV in $VioA_{O7}$ (Fig. 7). A glycine residue in motif II is replaced by a serine residue in $VioA_{O7}$, and the same was found in StsC and TbmB, the glutamine:*scyllo*-inosose aminotransferases from *Streptomycetes* (1, 14). A lysine residue in motif IV has been suggested to form a Schiff base with cofactor PLP (12). In $VioA_{O7}$, we found two arginine residues and one lysine residue in tandem at the site. As in lysine, arginine also contains the ε-NH_2 group and is expected to contribute to the binding of PLP. This may explain the higher activity of $VioA_{O7}$, which has a K_m value that is 20 times lower and a k_{cat}/K_m ratio that is about 150 times higher than those of $VioA_{D7}$. Furthermore, the K_m of $VioA_{O7}$ is the lowest among all kinetically characterized SATs, including Cj1294 (27), Cj1121c (36), WecE (12), and RfbE (2). In future work, it is worthwhile to perform site-directed mutagenesis at the potential active sites to investigate any significance of amino acid substitution in relation to enzyme activity.

Having the maximum activity at 37°C while losing most of the activity at higher temperatures (65°C and above) for $VioA_{D7}$, but not for $VioA_{O7}$, may reflect the different niches occupied by *Shigella* and *E. coli*. *Shigella* strains live only inside the human intestine, and *E. coli* strains can adapt to various environmental niches, either inside or outside the human body. The activity of $VioB_{O7}$ is also maintained over a wide temperature range.

Rare sugars are potentially useful in the pharmaceutical and chemical industries for drug development. Amino sugars have been reported as components of many macrolide antibiotics, including tylosin, desosamine, and erythromycin (7, 8, 23, 37). Chemical synthesis of rare sugars is difficult due to the need for multistep reactions of protection and deprotection. This work provides genetic and biochemical means for the synthesis of Qui4N and Qui4NAc, which are not commonly found and are not yet commercially available.

ACKNOWLEDGMENTS

We thank Dawei Zhou for technical assistance with RP-HPLC.

This work was supported by the NSFC General Program (grants 30370023, 30670038, and 30500024), the NSFC Key Program (grant 30530010), the Tianjin Municipal Special Fund for Science and Technology Innovation (grant 05FZZDSH00800), the National 863 Program of China (grant 2006AA020703), the RFBR (grants 05-04-48992 and 05-04-39015 to A.V.P. and Y.A.K.), the Council on Grants of the president's office of the Russian Federation for Support of Young Russian Scientists (project MK-157.2007.4) to A.V.P., and the Russian Science Support Foundation.

REFERENCES

1. **Ahlert, J., J. Distler, K. Mansouri, and W. Piepersberg.** 1997. Identification of *stsC*, the gene encoding the L-glutamine:*scyllo*-inosose aminotransferase from streptomycin-producing Streptomycetes. Arch. Microbiol. **168:**102–113.
2. **Albermann, C., and W. Piepersberg.** 2001. Expression and identification of the RfbE protein from *Vibrio cholerae* O1 and its use for the enzymatic synthesis of GDP-D-perosamine. Glycobiology **11:**655–661.
3. **Bastin, D. A., and P. R. Reeves.** 1995. Sequence and analysis of the O antigen gene (*rfb*) cluster of *Escherichia coli* O111. Gene **164:**17–23.
4. **Bax, A., and D. G. Davis** 1985. MLEV-17 based two-dimensional homonuclear magnetization transfer spectroscopy. J. Magn. Reson. **65:**355–360.
5. **Breazeale, S. D., A. A. Ribeiro, and C. R. Raetz.** 2003. Origin of lipid A species modified with 4-amino-4-deoxy-L-arabinose in polymyxin-resistant mutants of *Escherichia coli*. An aminotransferase (ArnB) that generates UDP-4-deoxyl-L-arabinose. J. Biol. Chem. **278:**24731–24739.
6. **Caroff, M., D. Karibian, J. M. Cavaillon, and N. Haeffner-Cavaillon.** 2002. Structural and functional analyses of bacterial lipopolysaccharides. Microbes Infect. **4:**915–926.
7. **Chen, F., G. M. Evins, W. L. Cook, R. Almeida, N. Hargrett-Bean, and I. K. Wachsmuth.** 1991. Genetic diversity among toxigenic and nontoxigenic Vibrio cholerae O1 isolated from the western hemisphere. Epidemiol. Infect. **107:**225–233.
8. **Dhillon, N., R. S. Hale, J. Cortes, and P. F. Leadlay.** 1989. Molecular characterization of a gene from *Saccharopolyspora erythraea* (*Streptomyces erythraeus*) which is involved in erythromycin biosynthesis. Mol. Microbiol. **3:**1405–1414.
9. **Erridge, C., E. Bennett-Guerrero, and I. Poxton.** 2002. Structure and function of lipopolysaccharides. Microbes Infect. **4:**837–851.
10. **Feng, L., J. Tao, H. Guo, J. Xu, Y. Li, F. Rezwan, P. Reeves, and L. Wang.** 2004. Structure of the *Shigella* dysenteriae 7 O antigen gene cluster and identification of its antigen specific genes. Microb. Pathog. **36:**109–115.
11. **Graninger, M., B. Kneidinger, K. Bruno, A. Scheberl, and P. Messner.** 2002. Homologs of the Rml enzymes from *Salmonella enterica* are responsible for dTDP-beta-L-rhamnose biosynthesis in the gram-positive thermophile *Aneurinibacillus thermoaerophilus* DSM 10155. Appl. Environ. Microbiol. **68:**3708–3715.
12. **Hwang, B. Y., H. J. Lee, Y. H. Yang, H. S. Joo, and B. G. Kim.** 2004. Characterization and investigation of substrate specificity of the sugar aminotransferase WecE from *E. coli* K12. Chem. Biol. **11:**915–925.
13. **Kharel, M. K., D. B. Basnet, H. C. Lee, K. Liou, J. S. Woo, B. G. Kim, and J. K. Sohng.** 2004. Isolation and characterization of the tobramycin biosynthetic gene cluster from *Streptomyces tenebrarius*. FEMS Microbiol. Lett. **230:**185–190.
14. **Kharel, M. K., B. Subba, H. C. Lee, K. Liou, and J. K. Sohng.** 2005. Characterization of L-glutamine:2-deoxy-scyllo-inosose aminotransferase (tbmB) from *Streptomyces tenebrarius*. Bioorg. Med. Chem. Lett. **15:**89–92.
15. **Kneidinger, B., S. Larocque, J. Brisson, N. Cadotte, and J. Lam.** 2003. Biosynthesis of 2-acetamido-2,6-dideoxy-L-hexoses in bacteria follows a pattern distinct from those of the pathways of 6-deoxy-L-hexoses. Biochem. J. **371:**989–995.
16. **Kneidinger, B., K. O'Riordan, J. Li, J. Brisson, J. Lee, and J. Lam.** 2003. Three highly conserved proteins catalyze the conversion of UDP-*N*-acetyl-D-glucosamine to precursors for the biosynthesis of O antigen in *Pseudomonas aeruginosa* O11 and capsule in *Staphylococcus aureus* type 5. J. Biol. Chem. **278:**3615–3627.
17. **Knirel, Y. A., V. V. Dashunin, A. S. Shashkov, N. K. Kochetkov, B. A. Dmitriev, and I. L. Hofman.** 1988. Somatic antigens of Shigella: structure of the O-specific polysaccharide chain of the *Shigella dysenteriae* type 7 lipopolysaccharide. Carbohydr. Res. **179:**51–60.
18. **Lerouge, I., and J. Vanderleyden.** 2002. O-antigen structural variation: mechanisms and possible roles in animal/plant-microbe interactions. FEMS Microbiol. Rev. **26:**17–47.
19. **L'vov, V. L., A. S. Shashkov, B. A. Dmitriev, N. K. Kochetkov, B. Jann, and K. Jann.** 1984. Structural studies of the O-specific side chain of the lipopolysaccharide from *Escherichia coli* O7. Carbohydr. Res. **126:**249–259.
20. **Marolda, C. L., M. F. Feldman, and M. A. Valvano.** 1999. Genetic organization of the O7-specific lipopolysaccharide biosynthesis cluster of *Escherichia coli* VW187 (O7:K1). Microbiology **145:**2485–2495.
21. **Matsuhashi, M., and J. L. Strominger.** 1966. Thymidine diphosphate 4-acetamido-4,6-dideoxyhexoses III. Purification and properties of thymidine diphosphate 4-keto-6-deoxy-D-glucose transaminase from *Escherichia coli* strain B. J. Biol. Chem. **241:**4738–4744.
22. **McNally, D., I. Schoenhofen, E. Mulrooney, D. Whitfield, E. Vinogradov, J. Lam, S. Logan, and J. Brisson.** 2006. Identification of labile UDP-ketosugars in *Helicobacter pylori*, *Campylobacter jejuni* and *Pseudomonas aeruginosa*: key metabolites used to make glycan virulence factors. Chem. Biol. Chem. **7:**1865–1868.
23. **Merson-Davies, L. A., and E. Cundliffe.** 1994. Analysis of five tylosin bio-

synthetic genes from the tylIBA region of the *Streptomyces fradiae* genome. Mol. Microbiol. **13:**349–355.
24. **Nakano, Y., N. Suzuki, Y. Yoshida, T. Nezu, Y. Yamashita, and T. Koga.** 2000. Thymidine diphosphate-6-deoxy-L-*lyxo*-4-hexulose reductase synthesizing dTDP-6-deoxy-L-talose from *Actinobacillus actinomycetemcomitans*. J. Biol. Chem. **275:**6806–6812.
25. **Nataro, J. P., and J. B. Kaper.** 1998. Diarrheagenic *Escherichia coli*. Clin. Microbiol. Rev. **11:**142–201.
26. **Niyogi, S. K.** 2005. Shigellosis. J. Microbiol. **43:**133–143.
27. **Obhi, R. K., and C. Creuzenet.** 2005. Biochemical characterization of the *Campylobacter jejuni* Cj1294, a novel UDP-4-keto-6-deoxy-GlcNAc aminotransferase that generates UDP-4-amino-4,6-dideoxy-GalNAc. J. Biol. Chem. **280:**20902–20908.
28. **Parolis, H., L. A. Parolis, and G. Olivieri.** 1997. Structural studies on the Shigella-like *Escherichia coli* O121 O-specific polysaccharide. Carbohydr. Res. **303:**319–325.
29. **Perepelov, A. V., D. Babicka, S. N. Senchenkova, A. S. Shashkov, H. Moll, A. Rozalski, U. Zahringer, and Y. A. Knirel.** 2001. Structure of the O-specific polysaccharide of Proteus vulgaris O4 containing a new component of bacterial polysaccharides, 4,6-dideoxy-4-{*N*-[(R)-3-hydroxybutyryl]-L-alanyl}amino-D-glucose. Carbohydr. Res. **331:**195–202.
30. **Pfoestl, A., A. Hofinger, P. Kosma, and P. Messner.** 2003. Biosynthesis of dTDP-3-acetamido-3,6-dideoxy-alpha-D-galactose in *Aneurinibacillus thermoaerophilus* L420-91T. J. Biol. Chem. **278:**26410–26417.
31. **Reeves, P. R.** 1995. Role of O-antigen variation in the immune response. Trends Microbiol. **3:**381–386.
32. **Reeves, P. R., and L. Wang.** 2002. Genomic organization of LPS-specific loci. Curr. Top. Microbiol. Immunol. **264:**109–135.
33. **Stenutz, R., A. Weintraub, and G. Widmalm.** 2006. The structures of *Escherichia coli* O-polysaccharide antigens. FEMS Microbiol. Rev. **30:**382–403.
34. **Stroeher, U. H., L. E. Karageorgos, M. H. Brown, R. Morona, and P. A. Manning.** 1995. A putative pathway for perosamine biosynthesis is the first function encoded within the *rfb* region of *Vibrio cholerae* O1. Gene **166:** 33–42.
35. **Sweet, C. R., A. A. Ribeiro, and C. R. Raetz.** 2004. Oxidation and transamination of the 3″-position of UDP-*N*-acetylglucosamine by enzymes from *Acidithiobacillus ferrooxidans*. Role in the formation of lipid a molecules with four amide-linked acyl chains. J. Biol. Chem. **279:**25400–25410.
36. **Vijayakumar, S., A. Merkx-Jacques, D. B. Ratnayake, I. Gryski, R. K. Obhi, S. Houle, C. M. Dozois, and C. Creuzenet.** 2006. Cj1121c, a novel UDP-4-keto-6-deoxy-GlcNAc C-4 aminotransferase essential for protein glycosylation and virulence in *Campylobacter jejuni*. J. Biol. Chem. **281:**27733–27743.
37. **Volchegursky, Y., Z. Hu, L. Katz, and R. McDaniel.** 2000. Biosynthesis of the anti-parasitic agent megalomicin: transformation of erythromycin to megalomicin in *Saccharopolyspora erythraea*. Mol. Microbiol. **37:**752–762.
38. **Yatsuyanagi, J., S. Saito, and I. Ito.** 2002. A case of hemolytic-uremic syndrome associated with Shiga toxin 2-producing *Escherichia coli* O121 infection caused by drinking water contaminated with bovine feces. Jpn. J. Infect. Dis. **55:**174–176.
39. **Yoshida, Y., Y. Nakano, T. Nezu, Y. Yamashita, and T. Koga.** 1999. A novel NDP-6-deoxyhexosyl-4-ulose reductase in the pathway for the synthesis of thymidine diphosphate-D-fucose. J. Biol. Chem. **274:**16933–16939.